ChemCatChem

The European Society Journal for Catalysis

Chemistry Europe

European Chemical Societies Publishing

Supported by GECATS GERMAN CATALYSIS SOCIETY

Accepted Article

Title: Revealing the Li2O2 nucleation mechanisms on CeO2 catalysts for lithium-oxygen batteries

Authors: Henry A. Cortes, María A. Barral, Nicola Seriani, Horacio R. Corti, and Veronica Vildosola

To be cited as: *ChemCatChem* 10.1002/cctc.202000013

Link to VoR: https://doi.org/10.1002/cctc.202000013

WILEY-VCH

FULL PAPER WILEY-VCH

Revealing the Li_2O_2 nucleation mechanisms on CeO_2 catalysts for lithium-oxygen batteries

Henry A. Cortes,[a] María A. Barral,[a] Nicola Seriani,[c] Horacio R. Corti,[ab] and Verónica L. Vildosola*[a]

[a] H.A. Cortes, Dr. M. A. Barral, Prof. H. R. Corti, Dr. V. L. Vildosola
Departamento de Física de la Materia Condensada
Instituto de Nanociencia y Nanotecnología (INN CNEA-CONICET)
Av. Gral Paz 1499, Partido de San Martín, Buenos Aires, Argentina.
E-mail: vildosol@tandar.cnea.gov.ar
[b] Prof. H. R. Corti
Instituto de Química Física de los Materiales Medio Ambiente y Energía (INQUIMAE CONICET)
Pabellón 2, Ciudad Universitaria, Buenos Aires Argentina.
E-mail: hrcorti@tandar.cnea.gov.ar
[c] Dr. N. Seriani
The Abdus Salam ICTP
Strada Costiera 11, I-34151 Trieste, Italy.
E-mail: nseriani@ictp.it.

Abstract: The addition of ceria (CeO_2) nanoparticles to the cathode of a lithium-oxygen battery results in increased capacity, lower overpotentials and better cyclability. To shed light on the mechanisms of this performance enhancement, we have investigated the early stages of Li_2O_2 nucleation at stoichiometric and reduced ceria surfaces by means of atomistic simulations based on density functional theory. Adsorption energies are stronger on ceria than on graphene, that is, nucleation mainly would take place on the oxide. The adsorption process of O_2 is the one that determines the nucleation sites for the Li_2O_2 formation on the different CeO_2 surfaces. The LiO_2 intermediate is adsorbed at the O_2 reduction sites. On the reduced (100) surface, the LiO_2 tends to adsorb dissociatively, opening up the possibility to the formation of other species than the desired end-product, Li_2O_2. On the contrary, optimal properties are found for the reduced (110) surface, which should therefore be the most active surface for Li_2O_2 nucleation among all low-index surfaces of ceria. These findings could pave the route to produce better cathodes for Li-oxygen batteries by the addition of carefully designed ceria nanoparticles, which maximizes the exposition of the most favourable facet.

Introduction

Despite the efforts for approaching in practice its high theoretical energy density, the deployment of Li–O_2 batteries (LOB) is hindered by many challenges. With reason, it has been suggested that, instead of simply sticking to performance improvements of LOBs, fundamental issues should be considered.[1] Among these issues are the effect of the solvent on the morphology and charge transport properties of the discharge product,[2,3] the use of redox mediators (liquid catalysts),[4-8] modifying the porosity of the carbon cathode,[7,8] and the use of noble metals and metal oxide catalysts.[8-13] In this work, we focus on ceria (CeO_2), a promising catalyst for LOBs,[14-17] with the aim to shed light on the mechanisms operating in the nucleation of Li_2O_2 at stoichiometric and reduced ceria surfaces by means of atomistic simulations based on density functional theory.

The growth mechanism of Li_2O_2 during the discharge of the non-aqueous Li-O_2 battery (LOB) varies depending on the donor number (DN) of the solvent.[2] When DN is high, there are more solvated LiO_2 species and the solution mechanism prevails, increasing the battery capacity but leading to the formation of large (toroidal shape) Li_2O_2 particles, whose re-dissolution during the recharge requires high over-potentials. On the other hand, when DN is low, O_2 is reduced to superoxide on the cathode surface where it combines with a Li^+ ion to form LiO_2 (adsorbed at the cathode surface), which reduces again or it disproportionates to form adsorbed Li_2O_2. Since Li_2O_2 is a large band gap insulator,[18] the charge transport occurs by tunneling through thin Li_2O_2 films (up to 10 nm thick), which limits the capacity of the battery, although it exhibits lower over-potential during recharge.[14]

As a way to circumvent this dichotomy, it has been recently shown experimentally that thicker films (non toroidal) can grow on small CeO_2 nanoparticles (NPs) added to carbon nanotubes (CNT), and the solution affinity of the solvent is increased through H_2O addition.[14] It was suggested that the nucleation enhancement by the CeO_2 NPs precludes the solution mechanism despite the increased donor number, forming a thin Li_2O_2 film. This is followed by the production of LiO_2, from ceria-free areas of the CNT, which disproportionates in solution forming Li_2O_2 deposits on the existing thin film, maintaining its shape. Also, the strong adsorption of LiO_2 at CeO_2 microspheres supported on graphene foam has proved to improve the LOB efficiency by avoiding its dissolution in the electrolyte and forming a uniform deposit of Li_2O_2.[16]

The well known catalytic activity of CeO_2, due to the formation of oxygen vacancies that result in the partial reduction of lattice cerium ions from Ce^{+4} to Ce^{+3}, together with reversibility of this process, facilitates both, the oxygen reduction reaction (ORR) and the oxygen evolution reaction (OER) during the discharge and charge of the LOB.[19]

It has been shown that the catalytic performance of ceria nanoparticles depends on its morphology and that the redox activity varies on the different exposed CeO_2 facets.[20-22] Even in the context of the LOB, it has been reported that NPs with film-like morphology exhibits higher capacity than octahedral and spherical ones.[23] However, no details are given regarding the different crystalline facets that are exposed in the reported NPs, and the higher capacity is explained in terms of higher surface area.

The energetic of the intermediates and precursors of the ORR at the reduced surfaces of CeO_2 (111) was recently studied.[24] It was concluded that the reaction path with the lithium adsorption as the first step was the most probable one, a fact that has not been experimentally confirmed yet.

Here we study, by resorting to DFT calculations, the first step of the surface Li_2O_2 formation analyzing the adsorption of O_2 and LiO_2 intermediates on both, stoichiometric and reduced (111), (110), and (100) surfaces, to evaluate the different catalytic activity in all the low index surfaces of CeO_2. In the context of this work, and from the technical point of view of DFT calculations, care should be taken while describing electrochemical processes that imply charged ions approaching insulating substrates. Our aim is to assess the nucleation power for Li_2O_2 of the different ceria facets, in order to suggest new routes to improve the catalytic efficiency of this catalyst in a LOB.

Details on the DFT calculations are described in the Computational methods section.

Results and Discussion

Recently, a volcano correlation was found between the discharge/charge voltage of the LOB and the LiO_2 adsorption on different metals.[25] It was shown that those metals with calculated adsorption energies for LiO_2 close to ~ -2.6 eV present a better performance, that is, a smaller discharge/charge overpotential. It was linked to smaller Li_2O_2 particle size of the discharge product. In the following, we will use these optimal values as a reference.[25,26]

In our DFT+U calculations, several adsorption sites were considered for each of the species. Along this work we will use the following notation: ST=stoichiometric, SOV=surface oxygen vacancy, and SSOV=subsurface oxygen vacancy.

In the Supplementary Information we report the calculated surface energies (Table S1) and oxygen vacancy formation energies (Table S4) for the most stable configurations of the three surface orientation considered for CeO_2.

Oxygen/lithium superoxo adsorption on the stoichiometric CeO_2 surfaces

In Figure 1, the most energetically stable configurations of O_2 and LiO_2 upon the ST (111), (110) and (100) facets are shown. Table 1 summarizes the corresponding adsorption energies (E_{ads}) and geometrical parameters for O_2 and LiO_2. The results for all the studied configurations are shown in the Supplementary Information (Tables and Figures S1-S3).

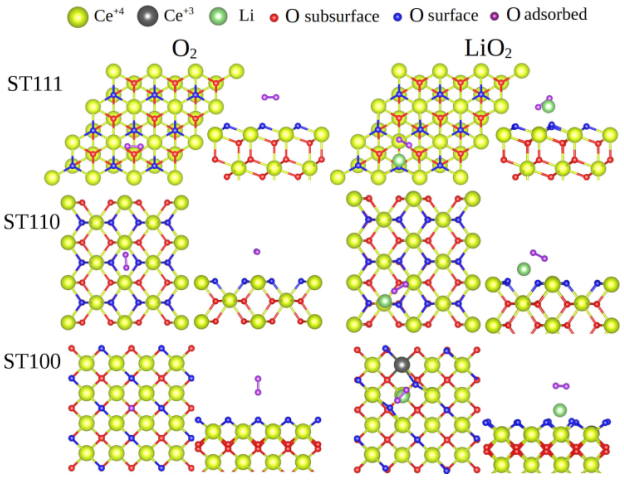

Figure 1: The most stable adsorbed configuration of O_2 and LiO_2 onto each ST CeO_2 facets, top and side view.

Table 1: E_{ads}, adsorbed height (h_{ads}) and the distance d_{O-O} between oxygens for the adsorbed O_2 and LiO_2 molecules on the ST (111), (110) and (100) facets.

Orientation	O_2			LiO_2		
	E_{ads} (eV)	h_{ads} (Å)	d_{O-O} (Å)	E_{ads} (eV)	h_{ads} (Å)	d_{O-O} (Å)
ST(111)	-0.10	2.69	1.23	-1.41	1.63	1.35
ST(110)	-0.16	2.80	1.24	-2.50	1.08	1.33
ST(100)	-0.08	2.49	1.23	-1.97	1.03	1.25

The valence state of the adsorbed oxygen molecule is assessed through the resulting O-O bonding length, d_{O-O}, upon reduction. That is, for the peroxide valence state O_2^{-2}, the superoxide O_2^- and the neutral oxygen molecule, the expected d_{O-O} are ~ 1.5 Å, ~ 1.3 Å and ~ 1.2 Å, respectively. It is worth to mention that the charged state of the molecules was confirmed by the calculated Bader charges as we show in the Supplementary Information (Table S8).

As it is known, the O_2 molecule adsorption on the ST facets is always a physical adsorption, with a weak adsorption energy and an adsorbed height between 2.49 and 2.80 Å. The O_2 molecule does not dissociate in any of the three ST facets and the oxygen bond-length is close to that of the neutral molecule (~ 1.2 Å). The O_2 adsorption orientation is similar in the ST (111) and ST (110) facets, where it remains in a lying position while it is perpendicular to the ST (100) surface. These results confirm previous studies,[21] indicating that superoxo and peroxo species of O_2 do not form in the low index facets of ST CeO_2.

It can also be observed in Figure 1 and Table 1, that in the ST (111) surface, the most stable adsorption energy of LiO_2 is -1.41 eV with an adsorption height of 1.63 Å, being this one, the weakest adsorption among the three facets. On the other hand, the ST (110) and ST (100) cases have adsorption energies of -2.50 eV and -1.97 eV, with similar adsorption heights. Resorting to the volcano behavior,[25] the ST (110) facet presents an adsorption energy that is very close to the one of the top of the volcano (-2.6 eV), indicating that it could have a good performance in the formation and decomposition of Li_2O_2.

Each facet shows a different adsorption orientation of the LiO_2 molecule, as depicted in Figure 1. For both, ST (111) and ST (110) facets, the LiO_2 is slightly tilted and the O_2 bond length is 1.35 Å, that corresponds to the superoxo species. On the other hand, at the ST (100) surface, the LiO_2 is basically dissociated, leading to adsorbed Li and the formation of one surface Ce^{+3}, meanwhile, the O_2 moves away with d_{O-O} = 1.25 Å, that is close to that of the neutral species.

These results show that the LiO_2 molecule can be adsorbed at the ST CeO_2 (111) and (110) surfaces, the last case presenting an adsorption energy which is very close to the optimal value of the volcano plot.[25] However, taking into account that O_2 does not get reduced at the stoichiometric CeO_2 surface, it should find alternatives paths to get reduced in order to form LiO_2, for instance through the solution mechanism at unpassivated areas of the carbon cathode close to the NPs.

Oxygen/lithium superoxo adsorption on the reduced CeO_2 surfaces

In this section, we will describe the adsorption of these intermediate species at the reduced CeO_2 surfaces.

Recently, a controversy has aroused on the stability of the SOV configuration in the (111) surface. On one hand, Sauer and coworkers[21] provided evidence for the formation of various

superoxo and peroxo species at single crystal O-vacancy sites on reduced CeO_2 (100) and (110) surfaces, but not on the reduced (111) one, which is the more stable surface orientation. Since the calculated formation energy of the oxygen vacancy in the subsurface is ~ 0.28 eV lower than the surface one, the absence of superoxo and peroxo formation at this particular facet is assigned to a subsurface diffusion of O vacancies. However, Schilling *et al*.[22] show through in situ Raman spectroscopy that in contrast to single crystals, the (111), truncated nanoparticles possess both surface and subsurface oxygen vacancies, and peroxides species do form at 35 ^{0}C.[22] Therefore, both vacancy configurations should be considered in the (111) facet if aiming to describe the effect of CeO_2 nanoparticles in the context of the LOB.

The calculated formation energies of the vacancies at each surface are presented in the Supplementary Information (see Table S4). It is important to remark, that despite the (111) orientation is the more stable one, the formation energy of the oxygen vacancy is lower in the (110) one, so that a higher concentration of Ce^{+3} is expected at this surface.

In Figure 2 we show the optimized adsorption configurations of O_2 and LiO_2 for the more stable situations in the SSOV (111), SOV (111), SOV (110) and SOV (100) facets. Table 2 summarizes the corresponding adsorption energies and geometrical parameters. Again, the results of the rest of the studied configurations are given in the Supplementary Information (Tables and Figures S5-S7).

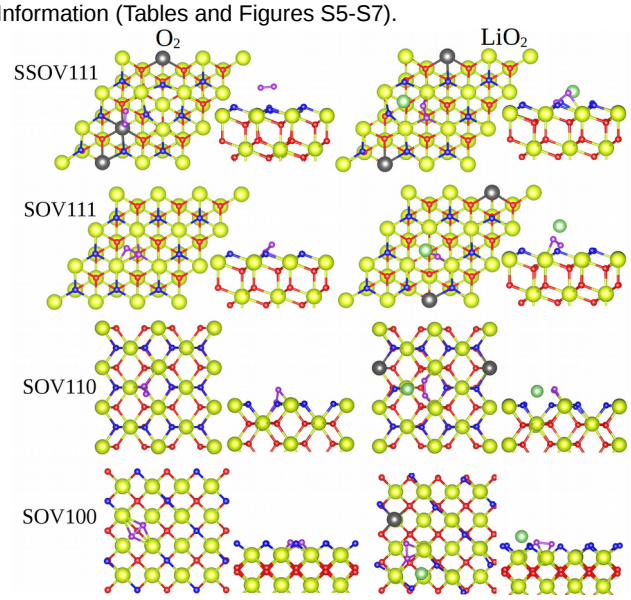

Figure 2: The most stable adsorbed configuration of O_2 and LiO_2 onto SSOV (111), SOV (111), SOV (110) and SOV (100) facets, top and side view.

Table 2: E_{ads}, h_{ads} and d_{O-O} of the adsorbed O_2 and LiO_2 molecules on the SSOV (111), SOV (111), SOV (110) and SOV (100) facets.

Orientation	O_2			LiO_2		
	E_{ads} (eV)	h_{ads} (Å)	d_{O-O} (Å)	E_{ads} (eV)	h_{ads} (Å)	d_{O-O} (Å)
SSOV(111)	-0.25	1.83	1.26	-3.12	-	1.46
SOV(111)	-2.03	-	1.44	-2.77	0.47	1.47
SOV(110)	-1.30	-	1.44	-2.98	1.37	1.47
SOV(100)	-2.03	-	1.47	-4.02	0.12	1.46

In the SOV (110) and SOV (100) cases, the O_2 prefers to fill the oxygen vacancy site and the bond length is increased from 1.23 Å to 1.44 and 1.47 Å, close to the characteristic bond length of the peroxo species. The O_2 reduction leads to the oxidation of a Ce^{+3} to Ce^{+4} (see Figure 2), in agreement with previous reported calculations.[22] The adsorption energies of the more stable situations in the (110) and (100) surfaces are -1.30 and -2.03 eV, respectively, in contrast to the SSOV (111) one where O_2 presents a physical adsorption with a bond height of 1.83 Å and a d_{O-O} bond length of 1.26 Å, close to the one of the neutral O_2, 1.23 Å. Furthermore, in this last case, the two Ce^{+3} remains at the surface, and the O_2 is not reduced, confirming previous results by Sauer and coworkers.[21]

Even when the SOV (111) surface orientation is not the more stable defect situation, we have also studied the O_2 and LiO_2 adsorption on the SOV (111) case because, as mentioned before, in truncated NPs is a plausible one.[22] The most stable adsorption structures of O_2 upon the SOV (111) surface are shown in Figure 2 and Table 2. In this surface, the O_2 also prefers to fill the SOV site increasing the d_{O-O} bond-length up to 1.44 Å (the peroxo bond-length), while two Ce^{+3} are oxidized to Ce^{+4} (see Figure 2).

In the SSOV (111), SOV (110) and SOV (100) facets the final d_{O-O} bond lengths of the more stable adsorbed LiO_2 molecules are 1.46 and 1.47 Å, close to the corresponding bond length of the peroxo species. The LiO_2 is reduced leaving only one Ce^{+3} at the surface (see Figure 2).[27]

In the SSOV (111), the LiO_2 is slightly tilt, and one of the oxygen's surface moves towards the subsurface vacancy site to fill it. In the SOV (110), the LiO_2 is in a flat-lying position with an adsorption height of 1.37 Å to the SOV site. On the other hand, in the SOV (100) case, the LiO_2 dissociates and the O_2^{-2} stays close to the vacancy site with an adsorption height of 0.12 Å and the Li is adsorbed farther from the O_2^{-2}.

Regarding the LiO_2 adsorption energy and resorting to the volcano plot,[25] the closest value to the top of the volcano plot obtained is for the SOV (110) surface with $E_{ads}(LiO_2)$ = - 2.98 eV, followed by the SSOV (111) with the $E_{ads}(LiO_2)$ = -3.12 eV, and then by the SOV (100) case with $E_{ads}(LiO_2)$ = -4.02 eV. Again, as with the stoichiometric surfaces, it should be remarked that O_2 does not get reduced at the SSOV (111) configuration. Therefore, in order to form LiO_2, the O_2 molecules should first find alternatives places to get reduced.

For the SOV (111) case, as in the previous ones, the LiO_2 is reduced in a peroxo situation and prefers to fill the SOV site while the adsorbed LiO_2 remains slightly tilt over the surface (see Figure 2). Despite the final LiO_2 adsorption configuration is similar for both, the SSOV and SOV defects of the (111) orientation, there is a difference of 0.35 eV in the adsorption energy, being the LiO_2 adsorption stronger on the SSOV than on the SOV surface. The LiO_2 adsorption in the SOV(111) facet is close to the optimal value of the volcano plot,[25] although the energetic indicates that the SOV vacancy site is expected to be scarcer.

It is worth to mention that either, in the stoichiometric or in the reduced CeO_2, after the molecular adsorptions, the bond O-O of the O_2 and LiO_2 intermediates never breaks. The stability of this bond in the different facets is a necessary condition for Li_2O_2 formation, and an indication that non desired side reactions are unlikely.

Another important remark is that the calculated adsorption sites of the O_2 molecule are the same as for the adsorbed LiO_2. In all the cases the adsorbed O_2 fills an oxygen vacancy and gets anchored there. This fact indicates that the initial O_2 reduction will determine the nucleation sites for Li_2O_2 formation within the surface mechanism at the ceria facet. This conclusion is at variance with the one by Li *et al*.,[24] that claim that Li^+ adsorption is the first step of the reaction path. In that work, the calculated adsorption energy of neutral Li was stronger than that of the

oxygen molecule. However, we believe that the adsorption energy of neutral Li does not account for the electrochemical process in which a charged Li is adsorbed at the surface.

Summarizing, the oxygen vacancy formation energy is lowest at the (110) surface, so that this orientation is expected to be more easily reduced than the others. This is important because, without vacancy sites at the surface, the O_2 molecule does not form peroxo nor superoxo species. On the other hand, the LiO_2 adsorption energy at the (110) facet is very close to the optimal value of the volcano plot.[25] Then, although the O_2 adsorption energy is stronger for the (100) facet, the LiO_2 dissociates there, so that no Li_2O_2 nucleation is expected at this particular orientation. Finally, the more stable reduced condition for the (111) surface is not reactive towards O_2 reduction because the vacancy sites are at the subsurface layer. That is why we conclude this (111) exposed plane is not the more reactive one. However, as reported by Schilling *et al*.,[22] surface vacancy sites can be present for non-single crystal truncated particles, and considering the calculated LiO_2 adsorption energies, the Li_2O_2 nucleation cannot be completely disregarded in this case. In view of all the above results we conclude that the (110) facet is the more suitable for the Li_2O_2 nucleation.

Lithium peroxide adsorption on the reduced (110) CeO_2 surface

In this section, we focus on the (110) facet and we study in detail the adsorption of the Li_2O_2 molecule on the SOV (110) surface at the more stable nucleation sites determined before by the O_2 and LiO_2 intermediates. In Figure 3, the final adsorbed Li_2O_2 molecule, with calculated adsorption energy -3.38 eV., is shown.

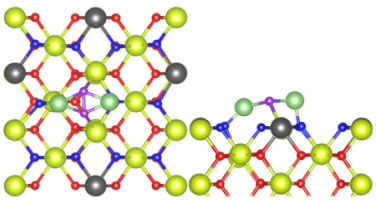

Figure 3: Optimized structure of Li_2O_2 on SOV (110) facet, top and side view.

In order to assess the nucleation power of ceria, we also calculate the adsorption of the Li_2O_2 molecule onto the (1-100) Li_2O_2 surface and graphene. We chose these particular cases firstly because the (1-100) Li_2O_2 surface is the more stable one, as we show in the Supplementary Information (Table S9 and Figure S9), so that it is expected to be the more abundant exposed facet of the already formed discharge product. Secondly, graphene is usually used as a reference cathode in several theoretical and experimental works.[14,15,28]

We obtained E_{ads}= -2.68 and -1.00 eV, for (1100) Li_2O_2 surface and graphene, respectively. The adsorption is clearly strongest at the SOV (110) CeO_2 surface. These results suggest, on one hand, that the Li_2O_2 prefers to be adsorbed onto ceria than on unpassivated regions of graphene, or on top of the existent Li_2O_2. On the other hand, this last fact implies that the amount of Li_2O_2 deposited in the form of large particles is not expected if ceria is present at the cathode.

There are other indications that support this conjecture. First, there are several sites where LiO_2 can be adsorbed on SOV (110) with similar adsorption energies (see Tables and Figures S6-S7). Second, the adsorption energy of a Li_2O_2 molecule on the SOV (110) surface is larger than the cohesive energy of bulk Li_2O_2 (E_{coh}= -3.27 eV). Finally, when we adsorb a second Li_2O_2 molecule, we observe that the less favorable configuration is that in which the second molecule is on top the first one. In view of all these facts, we conclude that Li_2O_2 might be prone to cover homogeneously the ceria surface rather that form large particles on it.

We also calculated the misfit factor $\eta = |1 - 2\Omega/(\Omega + A)|100\%$, as defined by Wang et al.[29] where Ω is the surface area of (110) CeO_2 surface and A is the surface area of the more stables (1100) and (0001) Li_2O_2 facets. We found a relative large η, of 7.55 and 9.41, respectively, as compared with other works, where the misfit between Li_2O_2 and TiC has been studied.[29,30] Therefore, we do not expect a high crystallinity of the Li_2O_2 deposited onto ceria.

Conclusions

We have studied the adsorption of O_2, LiO_2 and Li_2O_2 at the low index surfaces of CeO_2, both in stoichiometric and reduced conditions, by DFT. The adsorption process of O_2 will determine the nucleation sites for the Li_2O_2 formation on the different CeO_2 surfaces. In this respect, the SOV (100) surface exhibits a strongest adsorption energy for O_2, but our results indicate that the Li-O_2 bond breaks, in such a way that Li_2O_2 formation is not expected at this exposed plane.

On the other hand, the more stable configuration of the reduced CeO_2 (111) surface, is not reactive towards O_2 because the oxygen vacancy is at a subsurface site and, consequently, the nucleation power of this orientation is not expected to be high. However, the formation of O_2^- and O_2^{-2} species were reported in truncated nanoparticles[22] and they exhibit rather strong calculated O_2 adsorption energies, implying that the reactivity of this plane is not null.

The adsorption of LiO_2 molecule is the key intermediate step in the Li_2O_2 formation, and it is considered as a descriptor for the performance of a LOB. The adsorption of LiO_2 on the different CeO_2 surfaces studied is, in general, rather strong as compared to graphene. This behavior is in line with the experimental observation of a high nucleation power of ceria NPs deposited on graphene based cathodes.[14-17] In the adsorption process, the surface oxygen vacancy is filled, and the oxidation of Ce^{+3} to Ce^{+4} takes place.

Considering the optimal adsorption energy obtained of the LiO_2 molecule on the SOV (110) surface, together with a good reactivity for O_2, we conclude that this particular exposed plane presents better conditions as a catalyst for the LOB.

We propose that, in order to improve the efficiency of the catalyst, the exposure of the (110) NP facets should be maximized while the (100) one avoided. One possible route is the use of rod-shaped NPs (nanorods), which have been shown to expose mainly the face (110).[31-33]

These discoveries are crucial not only for enriching our understanding of the mechanism of ceria catalyst in the cathode of a LOB, but also provide direction for future promising research activities aimed at further enhancing the catalytic effect.

Computational details

Calculations were performed using density functional theory (DFT) with the projector augmented wave method (PAW) as implemented in the Vienna Ab initio Simulation Package (VASP).[34–36] The Coulomb interaction of occupied f orbitals is corrected via the DFT+U[37] approach employing the GGA-PBE[38] functional and an effective Hubbard-type U parameter of 5 eV. The DFT+U approach is necessary to account for the localized nature of the Ce-4f electrons.[39-41] A plane wave kinetic energy cutoff of 400 eV was used, and structures were optimized until forces acting on relaxed atoms were below 0.02 eVÅ^{-1}. Spurious interactions induced by dipole moments perpendicular to the surface are corrected with the dipolar correction.

The p(3x3), p(2x3) and c(2x2) surface unit cells studied in this work were generated by cutting bulk CeO_2 (lattice parameter a=5.435 Å obtained with DFT+U without Van der Waals corrections, in reasonable agreement with the experimental value of 5.411 Å[42]) in the (111), (110), and (100) orientations. The resulting slab models consist of 9, 7, and 11 atomic layers separated by a vacuum layer of 12 Å.[21,22]

The semi-empirical C_6/R_6 term parametrized by Grimme (DFT+D2)[43,44] was added to total energies and gradients, to correct for missing long-range dispersion-type interactions that might become relevant for some adsorbed species. Van der Waals parameters for Ce were previously derived and tested.[45]

The adsorption energies were calculated as:

$$E^{ads}=E_{slab+X} - (E_{slab} + E_X) \quad (1)$$

where E_{slab+X} is the total energy of the system, E_{slab} and E_X are the substrate and adsorbed species energies, separately.

To correct the known oxygen over-binding error, we employed the same approach as Cortes *et al*.,[46] obtaining a correction of 14 meV using DFT+D2.

The surface energies were calculated as:

$$E^{surf} =(E_{slab}-nE_{bulk})/2A \quad (2)$$

where E_{slab} is the total energy of the slab containing *n* formula units, E_{bulk} is the total energy per formula unit of bulk and *A* is the surface area of one of the two symmetric surfaces.

Acknowledgements

The authors thank financial support from ANPCyT (PICT 0869) and CONICET (PIP 2015 0364 GI). VLV, MAB, and HRC are members of CONICET. HACP thanks a fellowship from CONICET and the receipt of a fellowship from the ICTP short term visitor program, Trieste, Italy.

Conflict of Interest

The authors declare no conflict of interest.

Keywords: Cerium oxide catalyst • First principles calculations • Lithium-oxygen battery • Lithium peroxide nucleation.

[1] Y. Shao, F. Ding, J. Xiao, J. Zhang, W. Xu, S. Park, J. G. Zhang, Y. Wang, J. Liu, *Adv. Funct. Mater*.,**2012**, *23*, 987-1004.

[2] L. Johnson, C. Li; Z. Liu; Y. Chen, S. A. Freunberger, P. C. Ashok, B. B. Praveen; K. Dholakia, J. M. Tarascon, P. G. Bruce, *Nature Chem*. **2014**, *6*, 1091–1099.

[3] D. Sharon, D. Hirsberg, M. Salama, M. Afri, A. A. Frimer, M. Noked, W. Kwak, Y. K. Sun, D. Aurbach, *ACS Appl. Mater. Interfaces* **2016**, *8*, 5300-5307.

[4] J. B. Park, S. H. Lee, H. G. Jung, D. Aurbach, Y. K. Sun, *Adv. Mater*. **2018**, *30*, 1704162.

[5] C. M. Burke, R. Black, I. R. Kochetkov, V. Giordani, D. Addison, L. F. Nazar, B. D. McCloskey, *ACS Energy Lett***. 2016**, *1*, 747-756.

[6] V. Pande, V. Viswanathan, *ACS Energy Lett*. **2017**, *2*, 60-63.

[7] A. Dutta, R. A. Wong, W. Park, K. Yamanaka, T. Ohta, Y. Jung, H. R. Byon, *Nature Commun*. **2018**, *9*, 680.

[8] X. Q. Zhang, Ch. Z. Zhao, J. Q. Huang Q. Zhang. *Engineering.*, **2018**, 4, 831-847.

[9] E. Yilmaz; Ch. Yogi, K. Yamanaka, T. Ohta, H. R. Byon, *Nano Lett.* **2013**, *10*, 4679-4684.

[10] X. Guo, P. Liu, J. Han, Y. Ito, A. Hirata, T. Fujita, M. Chen, *Adv. Mater*. **2015**, *27*, 6137-6143.

[11] X. Li, Z. Liu, L. Song, D. Wang, Z. Zhang, *Electrochim. Acta* **2018**, *263*, 561-569.

[12] R. A. Wong, C. Yang, A. Dutta, M. O, M. Hong, M.; M. L. Thomas, K. Yamanaka, T. Ohta, K. Waki, H. R. Byon, *ACS Energy Lett.* **2018**, *3*, 592-597.

[13] Z, Liu, L. R. De Jesus, S. Banerjee, P. P. Mukherjee. *CS Appl. Mater. Interfaces.,* **2016**, 8, 23028-23036.

[14] C. Yang, R. A. Wong, M. Hong, K. Yamanaka, T. Ohta, H. R. Byon, *Nano Lett.* **2016**, *16*, 2969–2974.

[15] Y. Jiang, J. Cheng, L. Zou, X. Li, Y. Gong, B. Chi, J. Pu, J. Li, *Electrochim. Acta* **2016**, *210*, 712–719.

[16] Y. Jiang, J. Cheng, L. Zou, X. Li, Y. Huang, L. Jia, B. Chi, J. Pu, J. Li, *ChemCatChem* **2017**, *9*, 4231–4237.

[17] Y. Hou, J. Wang, Ch. Hou, Y. Fan, Y. Zhai, H. Li, F. Dang, Sh. Chou, *J. Mater. Chem. A*. **2019**, *11*, 6552-6561.

[18] M. D. Radin, D. J. Siegel, *Energy Environ. Sci*. **2013**, *6*, 2370–2379.

[19] T. Montini, M. Melchionna, M. Monai, P. Fornasiero, *Chem. Rev*. **2016**, *116*, 5987– 6041.

[20] L. Lin, S. Yao, Z. Liu, F. Zhang, N. Li, D. Vovchok, A. Martinez-Arias, R. Castaneda, J. Lin, S. D. Senanayake, D. Su, D. Ma, J. A. Rodriguez, *J. Phys. Chem. C* **2018**, *122*, 12934–12943.

[21] C. Yang, X. Yu, S. Heibler, P. G. Weidler, A. Nefedov, Y. Wang, C. Woll, T. Kropp, J. Paier, J. Sauer, *Angew. Chem. Int. Ed*. **2017**, *56*, 16399–16404.

[22] C. Schilling, M. V. Ganduglia-Pirovano, C. Hess, C. *J. Phys. Chem. Lett*. **2018**, *9*, 6593– 6598.

[23] X. Lin, L. Zhou, T. Huang, A. Yu, Int. J. Electrochem. Sci. **2012**, 7, 9550–9559.

[24] X. Li, Z. Li, X. Yang, L. Jia, Y. Q. Fu, B. Chi, J. Pu, J. Li, *J. Mater. Chem. A* **2017**, *5*, 3320–3329.

[25] Y. Yang, W. Liu, N. Wu, X. Wang, T. Zhang, L. Chen, R. Zeng, Y. Wang, J. Lu, L. Fu, L. Xiao, L. Zhuang, *ACS Appl. Mater. Interfaces* **2017**, *9*, 19800–19806.

[26] In order to compare our LiO_2 adsorption energies calculated for the different ceria surfaces with those reported in Ref. 25, we reproduced two of their calculations, the graphene [G] and platinum [Pt] (111) cases and obtained the adsorption energies -0.80 eV and -2.72 eV, respectively, in agreement with their reported values.

[27] The LiO_2 adsorbed molecule ends up in a peroxo situation. Even if it is expected that the two transferred electrons are taken from the surface, in this work, we always consider neutral supercells due to the technical difficulty of dealing with charged surfaces defects. So that we still have one Ce^{+3} at the surface after the molecule is adsorbed. We have checked that the calculated adsorption energy is not significally sensitive to the location of this spurious Ce^{+3}.

[28] Y. Yang, T. Zhang, X. Wang, L. Chen, N. Wu, W. Liu, H. Lu, L. Xiao, L. Fu, L. Zhuang, *ACS Appl. Mater. Interfaces* **2016**, *8*, 21350–21357.

[29] Z. Wang, X. Chen, Y. Cheng, C. Niu, *J. Phys. Chem. C* **2015**, *119*, 25684–25695.

[30] K. Raz, P. Tereshchuk, D. Golodnitsky, A. Natan, *J. Phys. Chem. C* **2018**, *122*, 16473–16480.

[31] Tana, M. Zhanga, J. Li, H. Li, Y. Li, W. Shen, *Catalysis Today*, **2009**, 148, 179-183.
[32] Ch. Li, Y. Sun, I. Djerdj, P. Voepel, C. Ch. Sack, T. Weller, R. Ellinghaus, J. Sann. Y. Guo, B. M. Smarsl, H. Over, *ACS Catal.*, **2017**, 7, 6453-6463.
[33] L. Lin, S. Yao, Z. Liu, F. Zhang, N. Li, D. Vovchok, A. M. Arias, R. Castañeda, J. Lin, S. D. Senanayake, D. Su, D. Ma, J. A. Rodriguez, *J. Phys. Chem. C.,* **2018**, 122, 12934-12943.
[34] G. Kresse, J. Furthmuller, *Comput. Mater. Sci.,* **1996**, *6*, 15–50.
[35] G. Kresse, J. Furthm¨uller, *Phys. Rev. B*, **1996**, *54*, 11169–11186.
[36] G. Kresse, D. Joubert, *Phys. Rev. B*, **1999**, *59*, 1758–1775.
[37] S. L. Dudarev, G. A. Botton, S. Y. Savrasov, C. J. Humphreys. A. P. Sutton, *Phys. Rev. B*, **1998**, *57*, 1505–1509.
[38] J. P. Perdew, K. Burke, M. Ernzerhof, *Phys. Rev. Lett*., **1996**, *77*, 3865–3868.
[39] B. Wang, X. Xi, A. N. Cormack, *Chem. Mater*., **2014**, *26*, 3687–3692.
[40] Y. Choi, M. Scott, T. Sohnel, H. Idriss, *Phys. Chem. Chem. Phys*., **2014**, *16*, 22588-22599.
[41] X. Li, Z. Li, X. Yang, L. Jia, Y. Q. Fu, B. Chi, J. Pu and J. Li, *J. Mater. Chem. A*, **2017**, *5*, 3320–3329.
[42] A. Filtschew, K. Hofmann, C. Hess, *J. Phys. Chem. C*, **2016**, *120*, 6694–6703.
[43] S. Grimme, *J. Comput. Chem.,* **2004**, *25*, 1463–1473.
[44] S. Grimme, *J. Comput. Chem*., **2006**, *27*, 1787–1799.
[45] C. Penschke, J. Paier, J. Sauer, *J. Phys. Chem. C*, **2013**, *117*, 5274–5285.
[46] H. A. Cortes, V. L. Vildosola, M. A. Barral, H. R. Corti, *Phys. Chem. Chem. Phys*., **2018**, *20*, 16924–16931.

Entry for the Table of Contents

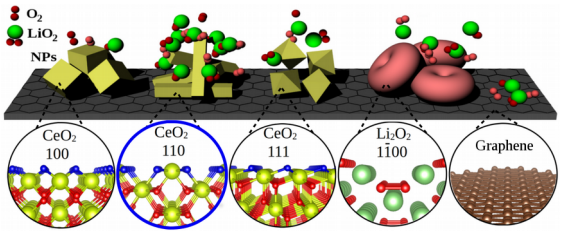

Ceria nanoparticles (NPs) added to the cathode improve the performance of the lithium-oxygen battery. In the early stages of Li_2O_2 nucleation at this catalyst, the adsorption energies are stronger than on graphene or the already formed Li_2O_2. The best catalytic conditions are found for the reduced (110) facet.